Two-way coupling of Thin Shell Finite Element Magnetic Models via an Iterative Subproblem Method

Vuong. Dang Quoc[1] and Christophe. Geuzaine[2]

[1]School of Electrical Engineering, Hanoi University of Science and Technology, Viet Nam
[2]ACE, Dept. of Electrical Engineering and Computer Science, University of Liege

Abstract

Purpose - This work deals with the correction of the inaccuracies near edges and corners arising from thin shell models by means of an iterative finite element subproblem method. The method is based on a thin shell solution in a complete problem, where conductive thin regions have been extracted and replaced by surfaces but strongly neglect errors on computation of the field distribution and Joule losses near edges and corners. **Design/Methodology/Approach -** This approach also allows a complete problem to define as a series subproblems (including inductors and magnetic or conducting regions, some of them being thin region), where each subproblem is influenced by all the others. For that, an iterative procedure between the subproblems must be required to obtain a convergence solution.

Finding - The method is based on a thin shell solution in a complete problem, where conductive thin regions have been extracted and replaced by surfaces but strongly neglect errors on computation of the field distribution and Joule losses near edges and corners.

Research limitations implications - This model is only limited to thin shell models by means of an iterative finite element subproblem method.

Originality/Value - The developed method is considered to couple SPs in two-way coupling correction, where each solution is influenced by all the others. This means that an iterative procedure between the SPs must be required to obtain an accurate (convergence) solution that defines as a series of corrections.

Keywords - Eddy current, magnetodynamics, finite element method, iterative subproblem method, thin shell.

1

1 Introduction

Thin shell (TS) models have been proposed by many authors in [1], [2] to avoid meshing volume thin regions (Fig.1, *left*) and are replaced by surfaces (Fig. 1, *right*) with interface conditions (ICs). But, these ICs ignore end and border effects, and lead to errors on the computation of local fields (such as eddy current density, magnetic forces and Joule losses) in the vicinity of geometrical discontinuities near edges and corners, increasing with the thickness. In order to cope with this challenge, many papers have recently proposed a subproblem method (SPM) for correcting inaccuracies near edges and corners appearing from the TS [3], [4], [11]. However, those were developed in one-way coupling correction, where no iteration between the subproblems (SPs) is required.

In this paper, the extended method is considered to couple SPs in two-way coupling correction, where each solution is influenced by all the others (Fig. 2). This means that an iterative procedure between the SPs must be required to obtain an accurate (convergence) solution that defines as a series of corrections.

The scenario of this method is based on a SP approach [3], [4], which consists in splitting a complete problem (consisted of stranded inductors and conducting magnetic and conductive thin regions) into multiple SPs that consider as a series of changes. This means that the complete solution is defined as the sum of the SP solutions. It can also speed up the calculation of variations of the

[1] The paper has been presented at the ISEF conference 2019, Nancy, France.

design. Each SP is influenced by other SPs via surface sources (SSs) or volume sources (VSs), where SSs are the changes of ICs through surfaces from SPs, and VSs are changes of permeability and conductivity material of volume thin regions. Each SP permits to make use of previous solutions for new problems instead of solving a new complete problem for each new set of parameters.

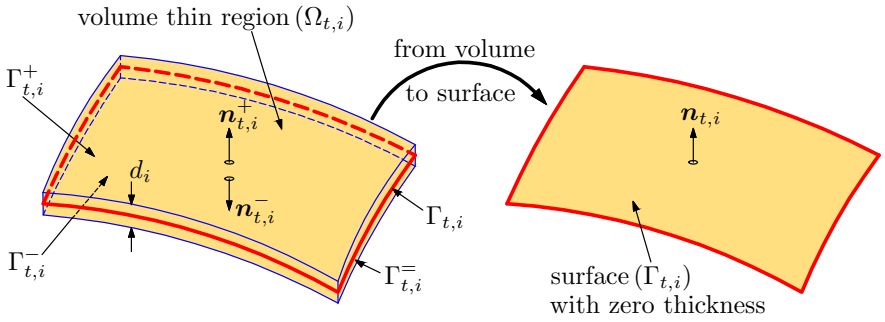

Fig. 1. Volume thin region Ω_t and surface Γ_t.

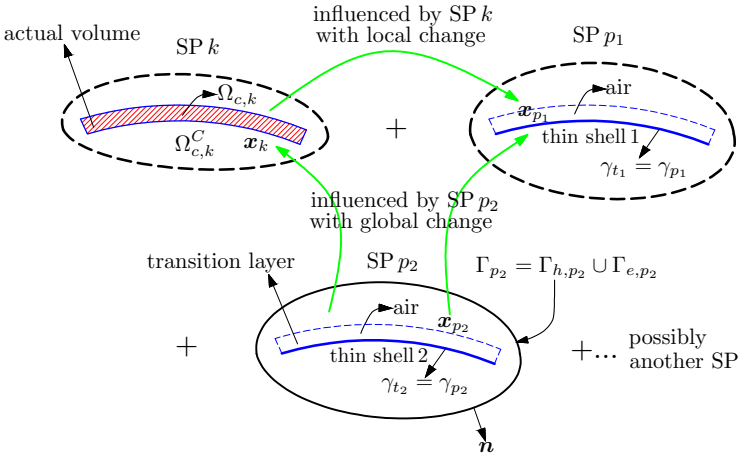

Fig. 2. Interative sequence of subproblems.

2 Definition of Subproblem Methodology

2.1 Canonical Magnetodynamic problem with VSs and SSs

A canonical magnetodynamic problem i, to be solved at step i of the heart SPM, is define in a domain Ω_i, with boundary $\partial\Omega_i = \Gamma = \Gamma_{h,i} \cup \Gamma_{e,i}$. The eddy current conducting part of Ω_i is denoted $\Omega_{c,i}$ and the non-conducting one $\Omega^{C}_{c,i}$, with $\Omega_c = \Omega_{c,i} \cup \Omega^{C}_{c,i}$. Stranded inductors belong to $\Omega^{C}_{c,i}$, whereas massive inductors is defined in $\Omega_{c,i}$. The equations, material relations and boundary conditions (BCs) of the SPs i are [3], [4]

$$\text{curl}\,\boldsymbol{h}_i = \boldsymbol{j}_i, \text{div}\boldsymbol{b}_i = 0, \text{curl}\boldsymbol{e}_i = -\partial_t \boldsymbol{b}_i \tag{1a-b-c}$$

$$\boldsymbol{h}_i = \mu_i^{-1}\boldsymbol{b}_i + \boldsymbol{h}_{s,i}, \boldsymbol{j}_i = \sigma_i \boldsymbol{e}_i + \boldsymbol{j}_{s,i} \tag{2a-b}$$

$$[\boldsymbol{n} \times \boldsymbol{h}_i]_{\Gamma_{h,i}} = \boldsymbol{j}_{f,i},\ [\boldsymbol{n} \cdot \boldsymbol{b}_i]_{\Gamma_{b,i}} = \boldsymbol{b}_{f,i}, [\boldsymbol{n} \times \boldsymbol{e}_i]_{\Gamma_{b,i}} = \boldsymbol{k}_{f,i} \tag{3a-b-c}$$

$$\boldsymbol{n} \times \boldsymbol{h}_i|_{\Gamma_{h,i}} = 0,\ \boldsymbol{n} \cdot \boldsymbol{b}_i|_{\Gamma_{b,i}} = 0, \tag{4a-b}$$

where $\boldsymbol{n}$ is the unit normal exterior to Ω_i, $\boldsymbol{b}_i$ is the magnetic flux density, $\boldsymbol{h}_i$ is the magnetic field, $\boldsymbol{j}_i$ is the electric current density,

$\boldsymbol{e}_i$ is the electric field, μ_i is the electric field, σ_i is the electric conductivity. The fields $\boldsymbol{h}_{s,i}$ and $\boldsymbol{j}_{s,i}$ in (2 a-b) are VSs, and the surface fields $\boldsymbol{j}_{f,i}$, $\boldsymbol{b}_{f,i}$ and $\boldsymbol{k}_{f,i}$ in (3 a-b-c) are SSs. It should be noted that SSs are generally zero for classical homogeneous BCs. ICs can define their discontinuities through any interface γ_i (with sides γ_i^+ and γ_i^-) in Ω_i, with the notation $[\cdot]_{\gamma_i} = |_{\gamma_i^+} - |_{\gamma_i^-}$. If nonzero, they define possible SSs that account for particular phenomena occurring at the idealized thin regions between γ_i^+ and γ_i^- [4]-[7].

2.2 Sequence of two-way coupling SPs

The solution $\boldsymbol{x}$ ($\boldsymbol{x} \equiv \boldsymbol{h}, \boldsymbol{b}, \boldsymbol{e}, \boldsymbol{j}, \ldots$) of complete problem is defined as the sum of SP solutions $\boldsymbol{x}_i$ achieved from different SPs [3], [4]. An appropriate series of SPs is defined via successive model refinements of an initially simplified problem. For an ordered set *P* of SPs, the summation of their solutions gives the total solution, i.e.

$$\boldsymbol{x} = \sum_{i \in P} \boldsymbol{x}_i \text{ with } \boldsymbol{x} \equiv \boldsymbol{h}, \boldsymbol{b}, \boldsymbol{e}, \boldsymbol{j}, \ldots \tag{5}$$

Each SP is solved in a simplified mesh and constrained via VSs in (2 a-b) and SSs in (3 a-b-c).

As discussed in the previous section, each SP *i* is influenced by all the other SPs *q* in *P*, i.e. all the SPs are coupled. This mean that SP *i* is usually grater than SP *q* ($i > q$) with the defined series. If $i < q$, this is the case when a correction becomes a significant source for any of its source SPs, which is inherent to large problems. These dependencies require procedure iterations on the set *P* to calculate each solution $\boldsymbol{x}_i$ as a series of corrections $\boldsymbol{x}_{i,j}$, i.e [11].

$$\lim_{n \to \infty} \boldsymbol{x}_i^n = \boldsymbol{x}_i = \sum_{j=1}^{n} \boldsymbol{x}_{i,j}. \tag{6}$$

The total solution at iteration *n* is thus

$$\boldsymbol{x}^n = \sum_{i \in P} \boldsymbol{x}_i^n = \sum_{i \in P} \sum_{j=1}^{n} \boldsymbol{x}_{i,j}. \tag{7}$$

The error ϵ^n of a solution $\boldsymbol{x}^n$ is defined by

$$\epsilon^n = \frac{||\boldsymbol{x}^n - \boldsymbol{x}_{\text{reference}}||}{||\boldsymbol{x}_{\text{reference}}||}, \tag{8}$$

where $\boldsymbol{x}_{\text{reference}}$ is a reference solution obtained from a finite element method. However, the reference solution is usually not known in advance. Thus, an estimated error $\epsilon^n_{\text{estimted}}$ of a solution $\boldsymbol{x}^n$ at iteration *n* has to be defined, e.g. as

$$\epsilon^n_{\text{estimted}} = \frac{||\boldsymbol{x}^n - \boldsymbol{x}^{n-1}||}{||\boldsymbol{x}^n||}. \tag{9}$$

The computation of the corrections $\boldsymbol{x}_{i,j}$ in a SP *i, j* (SP *i* with special constraints at iteration *n*) is maintained until convergence up to an expected accuracy. Each correction is under the influence of all the previous corrections $\boldsymbol{x}_{i,j}$ of other SPs, with *j* the last iteration index for which a correction is known, i.e. $j = n$ or n-1. Initial solutions x_i^0 are considered as zero.

3 Contraint between subproblems

3.1 Constraint between SPs with VSs

For changes in a region, form μ_q and σ_q for problem *q* to μ_p and σ_p for problem *p*, the VSs $\boldsymbol{h}_{s,i}$, and $\boldsymbol{j}_{s,i}$ in (2 a-b) are defined [3]-[5]

$$\boldsymbol{h}_{s,p} = (\mu_p^{-1} - \mu_q^{-1})\boldsymbol{b}_q, \qquad \boldsymbol{j}_{s,p} = (\sigma_p - \sigma_q)\boldsymbol{e}_q, \tag{10 a – b}$$

for the total fields to be related by the uploaded relations $\boldsymbol{h}_p + \boldsymbol{h}_q = \mu_p^{-1}(\boldsymbol{b}_p + \boldsymbol{b}_q)$ and $\boldsymbol{j}_p + \boldsymbol{j}_q = \sigma_p(\boldsymbol{e}_p + \boldsymbol{e}_q)$. A generalization of (4 a-b) to any number of source SPs has

$$\boldsymbol{h}_{s,p} = (\mu_p^{-1} - \mu_q^{-1}) \sum_{r\in P, r\neq p} \boldsymbol{b}_r\,, \qquad \boldsymbol{j}_{s,p} = (\sigma_p - \sigma_q) \sum_{r\in P, r\neq p} \boldsymbol{e}_r\,, \tag{11 a – b}$$

where q is the last solved SP. All the SPs $r \in P$ except the current one (q) contribute to the sources $\boldsymbol{h}_{s,p}$ and $\boldsymbol{j}_{s,p}$ via their last computed corrections $\boldsymbol{b}_r$ and $\boldsymbol{e}_r$.

In order to avoid the meshing of some regions, it can ignore changes from μ_q to μ_p in these regions with no sources (i.e., $\boldsymbol{h}_{s,p}$ =0 and $\boldsymbol{j}_{s,p}$=0) in (4 a-b) and (5). The material relations for the total files in such regions are thus

$$\boldsymbol{h}_p + \boldsymbol{h}_q = \mu_q^{-1}\boldsymbol{b}_q + \mu_p^{-1}\boldsymbol{b}_p, \quad \boldsymbol{j}_p + \boldsymbol{j}_q = \sigma_q\boldsymbol{e}_q + \sigma_p\boldsymbol{e}_p, \tag{12 a – b}$$

that can be transformed, with (5) particularized to $\boldsymbol{h}$ and $\boldsymbol{b}$, and to $\boldsymbol{j}$ and $\boldsymbol{e}$ i.e.,

$$\boldsymbol{h}_p = \mu_p^{-1}\boldsymbol{b}_p + (\mu_p^{-1} - \mu_q^{-1})\boldsymbol{b}_q, \qquad \boldsymbol{j}_p = \sigma_p\boldsymbol{e}_p + (\sigma_p - \sigma_q)\boldsymbol{e}_q. \tag{13 a – b}$$

It should be noted that the correction relations $\boldsymbol{h}_p = \mu_p^{-1}\boldsymbol{b}_p$ and $\boldsymbol{j}_p = \sigma_p\boldsymbol{e}_p$ are only rigorously fulfilled in the regions where μ and σ do not vary, with $\mu_p = \mu_q$ and $\sigma_p = \sigma_q$ [5].

3.2 Constraint between SPs with SSs

The constraint between SPs in the TS model is defined via SSs. This has done for the $\boldsymbol{b}_p$- formulation, requires a unknown discontinuity of $\boldsymbol{a}_{d,t,i}$ of the tangential component $\boldsymbol{a}_{t,i} = (\boldsymbol{n}\times\boldsymbol{a}_i)\times\boldsymbol{n}$ of $\boldsymbol{a}_{d,t,i}$ through TS, that is [1],

$$[\boldsymbol{a}_{t,i}]_{\Gamma_{ts,i}} = \boldsymbol{a}_{d,t,i} \text{ or } [\boldsymbol{n}\times\boldsymbol{a}_{t,i}]_{\Gamma_{ts,i}} = \boldsymbol{a}_{t,i}, \tag{14}$$

where $\boldsymbol{a}_{d,t,i}$ is the discontinuous component of the field $\boldsymbol{a}_{d,i}$ and is equal to zero on the negative side $\Gamma_{ts,i}^-$ of the TS, which cancels the magnetic flux entering there. In order to explicitly present the field discontinuity, it has [1]

$$\boldsymbol{a}_i|_{\Gamma_{ts,i}^+} = \boldsymbol{a}_{c,i} + \boldsymbol{a}_{d,,i}, \; \boldsymbol{a}_i|_{\Gamma_{ts,i}^-} = \boldsymbol{a}_{c,i}, \tag{15}$$

where $\boldsymbol{a}_{c,i}$ is the continuous component $\boldsymbol{a}_i$. The fields $\boldsymbol{a}_i$ and $\boldsymbol{a}_{d,t,i}$ are the tangential component defined on $\Gamma_{ts,i}$. In addition, SSs are defined via the BCs and ICs of impedance-type boundary conditions (IBC) combined with solutions from previous problem that can be also a stranded or massive inductor alone. In order to get a relative SS between SP q and current SP p ($i \equiv p$) via the corresponding ICs with $\gamma_t = \gamma_t^{\pm} = \gamma_q^{\pm} = \gamma_p^{\pm}$ and $\boldsymbol{n}_t = -\boldsymbol{n}$ for the TS, it must be figured that there is no thin region in SP i ($i \equiv q$). Therefore, one defines [1]

$$[\boldsymbol{n}\times\boldsymbol{h}_q]_{\gamma_q} = \boldsymbol{n}\times\boldsymbol{h}_q|_{\gamma_q^+} - \boldsymbol{n}\times\boldsymbol{h}_q|_{\gamma_q^+} = 0, \tag{16}$$

$$[\boldsymbol{n}\times\boldsymbol{h}]_{\gamma_p} = [\boldsymbol{n}\times\boldsymbol{h}_q]_{\gamma_p} + [\boldsymbol{n}\times\boldsymbol{h}_p]_{\gamma_p} = -\sigma\beta\partial_t(2\boldsymbol{a}_c + \boldsymbol{a}_d), \tag{17}$$

$$\boldsymbol{n}\times\boldsymbol{h}_p|_{\gamma_p^+} = \frac{1}{2}\left[\sigma\beta\partial_t(2\boldsymbol{a}_c + \boldsymbol{a}_d) + \frac{1}{\mu\beta}\boldsymbol{a}_d\right] - \boldsymbol{n}\times\boldsymbol{h}_q|_{\gamma_p^+} = \frac{1}{2}\left[\sigma\beta\partial_t(2\boldsymbol{a}_c + \boldsymbol{a}_d) + \frac{1}{\mu\beta}\boldsymbol{a}_d\right] - \boldsymbol{j}_f \tag{18}$$

$$\beta = \gamma^{-1}\tanh\left(\frac{d\gamma}{2}\right),\ \ \gamma = \frac{1+j}{\delta},\ \ \ \delta = \sqrt{\frac{2}{\omega\mu\sigma}} \tag{19}$$

where d is the local TS thickness, δ is the skin depth in the TS, $\omega = 2\pi f$ with f is the frequency, j is the imaginary unit and $\partial_t \equiv j\omega$. The discontinuity $[\boldsymbol{n}\times\boldsymbol{h}_q]_{\gamma_p}$ in (17) is equal to zero (i.e. $[\boldsymbol{n}\times\boldsymbol{h}]_{\gamma_p} = [\boldsymbol{n}\times\boldsymbol{h}_q]_{\gamma_q} + [\boldsymbol{n}\times\boldsymbol{h}_q]_{\gamma_p} = 0$) because there is no such discontinuity on the solution SP q.

4 Finite Element Weak Formulation

4.1 Magnetic Vector Potential Formulation

The weak $\boldsymbol{b}_i$-formulation (i $\equiv\ q,p,k$) for SPs i is obtained from the weak form ò the Ampere's law (1a), i.e. [3] - [7].

$$(\mu_i^{-1}\text{curl}\,\boldsymbol{a}_i, \text{curl}\,\boldsymbol{a}_i')_{\Omega_i} + (\sigma_i\partial_t\boldsymbol{a}_i, \boldsymbol{a}_i')_{\Omega_i} + (\sigma_i\text{grad}\,\nu_i, \boldsymbol{a}_i')_{\Omega_{c,i}} + (\boldsymbol{h}_{s,i}, \text{curl}\,\boldsymbol{a}_i')_{\Omega_{c,i}} + (\boldsymbol{j}_{s,i}, \text{curl}\,\boldsymbol{a}_i')_{\Omega_{c,i}} + \langle\boldsymbol{n}\times\boldsymbol{h}_i, \boldsymbol{a}_i'\rangle_{\Gamma_{h,i}}$$
$$+ \langle\boldsymbol{n}\times\boldsymbol{h}_i, \boldsymbol{a}_i'\rangle_{\Gamma_{b,i}} + \langle[\boldsymbol{n}\times\boldsymbol{h}_i]_{\gamma_i}, \boldsymbol{a}_i'\rangle_{\gamma_i} = +(\boldsymbol{j}_{s,i}\ \boldsymbol{a}_i')_{\Omega_{s,i}}, \forall\boldsymbol{a}_i' \in F_i^1(\Omega_i), \tag{20}$$

where $F_i^1(\Omega_i)$ is a gauged curl-conform function space defined on Ω_i, gauged in $\Omega_{c,i}^C$, and containing the basis functions for $\boldsymbol{a}_i$ as well as for the test function $\boldsymbol{a}_i'$ (at the discrete level, this space is defined by edge FEs; the gauge is based on the tree-cotree technique); $(.,.)_{\Omega_i}$ and $\langle.,.\rangle_{\Gamma_i}$ respectively denote a volume intergal in Ω_i and a surface intergal on Γ_i of the product of their vector field arguments. The surface integral term on $\Gamma_{h,i}$ accounts for natural BCs of type (4a), usually zero. The unknown term on the surface $\Gamma_{b,i}$ with essential BCs on $\boldsymbol{n}\cdot\boldsymbol{b}_i$ is often omitted because it does not locally contribute to (20). It will be shown the key for the post-processing a solution, a part of which $\boldsymbol{n}\times\boldsymbol{h}_i|_{\Gamma_{b,i}}$ having to act further as a SS [3], [4].

4.2 Subproblem with TS Models

The TS model [1] appeared in (20) is defined via the discontinuous term $\langle[\boldsymbol{n}\times\boldsymbol{h}_p]_{\gamma_p}, \boldsymbol{a}_p'\rangle_{\gamma_p}$ and is analyzed as:

$$\langle[\boldsymbol{n}\times\boldsymbol{h}_p]_{\gamma_p}, \boldsymbol{a}_p'\rangle_{\gamma_p} = \langle[\boldsymbol{n}\times\boldsymbol{h}_p]_{\gamma_p}, \boldsymbol{a}_c' + \boldsymbol{a}_d'\rangle_{\gamma_p} = \langle[\boldsymbol{n}\times\boldsymbol{h}_p]_{\gamma_p}, \boldsymbol{a}_c'\rangle_{\gamma_p} + \langle[\boldsymbol{n}\times\boldsymbol{h}_p]_{\gamma_p}, \boldsymbol{a}_d'\rangle_{\gamma_p}, \tag{21}$$

where $\boldsymbol{a}_d'$ and $\boldsymbol{a}_c'$ are the test functions; $\boldsymbol{a}_d'$ is defined as equal to zero on the negative side $\Gamma_{t,p}^- = \gamma_{t,p}^-$ of the TS [1]. For that, the equation (21) can be also rewritten as

$$\langle[\boldsymbol{n}\times\boldsymbol{h}_p]_{\gamma_p}, \boldsymbol{a}_p'\rangle_{\gamma_p} = \langle[\boldsymbol{n}\times\boldsymbol{h}_p]_{\gamma_p}, \boldsymbol{a}_c'\rangle_{\gamma_p} + \langle\boldsymbol{n}\times\boldsymbol{h}_p|_{\gamma_p^+}, \boldsymbol{a}_d'\rangle_{\gamma_{p^+}}. \tag{22}$$

The $\boldsymbol{h}_i$ trace discontinuity $\langle[\boldsymbol{n}\times\boldsymbol{h}_p]_{\gamma_p}, \boldsymbol{a}_c'\rangle_{\gamma_p}$ in (21) is given by (17), i.e.

$$\langle[\boldsymbol{n}\times\boldsymbol{h}]_{\gamma_p}, \boldsymbol{a}_c'\rangle_{\gamma_p} = \langle[\boldsymbol{n}\times\boldsymbol{h}_p]_{\gamma_p}, \boldsymbol{a}_c'\rangle_{\gamma_p} = \langle[\boldsymbol{n}\times\boldsymbol{h}_p]_{\gamma_p}, \boldsymbol{a}_c'\rangle_{\gamma_p} = \langle\sigma\beta\partial_t(2\boldsymbol{a}_c + \boldsymbol{a}_d), \boldsymbol{a}_c'\rangle_{\gamma_p}. \tag{23}$$

The surface integral term $\langle\boldsymbol{n}\times\boldsymbol{h}_p|_{\gamma_p^+}, \boldsymbol{a}_d'\rangle_{\gamma_{p^+}}$ in (22) applied on the positive side of the TS is given by (16), extracting the term $\boldsymbol{n}\times\boldsymbol{h}_q|_{\gamma_p^+}$ of the previous SP q and inserting the actual TS BC. Therefore, the resulting term $\langle\boldsymbol{n}\times\boldsymbol{h}_q|_{\gamma_p^+}, \boldsymbol{a}_d'\rangle_{\gamma_{p^+}}$ is a SS ($\boldsymbol{j}_f$) that can be correctly expressed via the weak formulation of SP q in (20), i.e.

$$-\langle\boldsymbol{n}\times\boldsymbol{h}_p|_{\gamma_p^+}, \boldsymbol{a}_d'\rangle_{\gamma_{p^+}} = (\mu_q^{-1}\text{curl}\,\boldsymbol{a}_q, \text{curl}\,\boldsymbol{a}_d')_{\Omega_{q^+=\Omega_{p^+}}} = -\boldsymbol{j}_f. \tag{24}$$

The contribution in the volume integral in (24) is limited to a single layer of FEs on the positive side of $\Omega_{q^+} = \Omega_{p^+}$ touching $\gamma_{p^+} = \gamma_{q^+}$ (Fig. 3), because it involves only the traces $\boldsymbol{a}'_d|_{\gamma_p^+}$. Substituting (24) and (23) into (20), one has the weak form of SP *p*. At the discrete level, the source $\boldsymbol{a}_q$, initially in mesh of SP *q*, has to be projected in mesh of SP *p* via a projection method [4], [8].

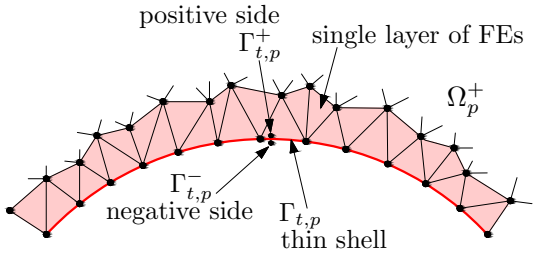

Fig. 3. Transition layer for TS SP *p*.

4.3 Subproblem with Actual Volume Corrections

The solutions achieved from previous SPs (SP *q* and SP *p*) are now considered as VSs for volume correction SP *k*, where the VSs are already given by (11 a) and (11 b). Of course, these sources will be also transferred from the mesh of the SP *q* and SP *p* to the mesh of current SP (SP *k*) via a projection method [4], [8]. Since that, the weak form for SP *k* is then defined as

$$(\mu_k^{-1}\operatorname{curl}\boldsymbol{a}_k, \operatorname{curl}\boldsymbol{a}'_k)_{\Omega_k} + (\sigma_k\partial_t\boldsymbol{a}_k, \boldsymbol{a}'_k)_{\Omega_{c,k}} + (\sigma_k\operatorname{grad}v_k, \boldsymbol{a}'_k)_{\Omega_{c,k}} + ((\mu_k^{-1} - \mu_p^{-1})(\operatorname{curl}\boldsymbol{a}_p + \operatorname{curl}\boldsymbol{a}_q), \operatorname{curl}\boldsymbol{a}'_k)_{\Omega_k}$$
$$+ \langle[\boldsymbol{n}\times\boldsymbol{h}_k]_{\gamma_{t,k}}, \boldsymbol{a}'_k\rangle_{\gamma_{t,k}} + (\sigma_k\partial_t(\boldsymbol{a}_q + \boldsymbol{a}_p), \boldsymbol{a}'_k)_{\Omega_{c,k}} = 0, \qquad \forall\boldsymbol{a}'_k \in F_k^1(\Omega_k). \tag{25}$$

At the same time to the VSs in (20), SSs in (25) have to reject the TS discontinuities, with ICs to be defined as

$$[\boldsymbol{n}\times\boldsymbol{h}_k]_{\gamma_{t,k}} = -[\boldsymbol{n}\times\boldsymbol{h}_p]_{\gamma_{t,k}} \text{ and } [\boldsymbol{n}\times\boldsymbol{a}_k]_{\gamma_{t,k}} = -[\boldsymbol{n}\times\boldsymbol{a}_p]_{\gamma_{t,k}}, \tag{26 a − b}$$

respectively in weak and strong senses, i.e. via a surface integral in the function $\$F_k^1(\Omega_k)$. The IC in (26 b) strongly fixes $\boldsymbol{a}_{d,t,k} = -\boldsymbol{a}_{d,t,p}$. The IC in (26 a) is weakly expressed through the term $-\langle[\boldsymbol{n}\times\boldsymbol{h}_k]_{\gamma_{t,k}}, \boldsymbol{a}'_k\rangle_{\gamma_p}$ in (25), with $\Gamma_p = \Gamma_k$. For that, the trace discontinuity $[\boldsymbol{n}\times\boldsymbol{h}_k]_{\gamma_{t,k}}$ occurred in (25) is defined via

$$\langle[\boldsymbol{n}\times\boldsymbol{h}_k]_{\gamma_{t,k}}, \boldsymbol{a}'_k\rangle_{\gamma_p} = -\langle[\boldsymbol{n}\times\boldsymbol{h}_p]_{\gamma_{t,k}}, \boldsymbol{a}'_k\rangle_{\gamma_p}. \tag{27}$$

and can be weakly evaluated from a volume integral SP *k* similar to (25). At the discrete level, these integrals are limited to the layers of FEs on both sides of TS, because they involve only the associated trace $\boldsymbol{n}\times\boldsymbol{a}'_k|_{\Gamma_{t,k}}$.

5 Application Test

A test problem is given in Fig. 4, for f = 50 Hz and 300 Hz, $\mu_r = 1$ and σ = 59 MS/m. The test is herein solved with five SPs, where three SPs (i.e. SP *q*, SP *p* and SP *k*) are already known from the one-way coupling example [3], [4].

A simplified problem SP *q* with the stranded inductor alone is first solved, then a TS FE SP p_1 is added without including the stranded inductor anymore. A volume correction SP k_1 covering the plate 1 then replaces the TS S p_1. Next, the second TS p_2 is inserted. The second volume correction SP k_2 covering the plate 2 finally replaces the TS SP p_2. In the correction strategy of SP p_1, the fields generated by SP p_2 and SP k_2 are reaction fields that influence the source solutions obtained from previous p_1. Hence, some iterations between the SPs are required to determine an accurate solution defined as a series of corrections. The iterative process is repeated until obtaining a convergence solution. There are herein two considerations: the first consideration is that the problem is

solved on the same mesh supporting to avoid an additional error due to mesh-to-mesh projections, and then it is tested on the different meshes taking the projection errors into account.

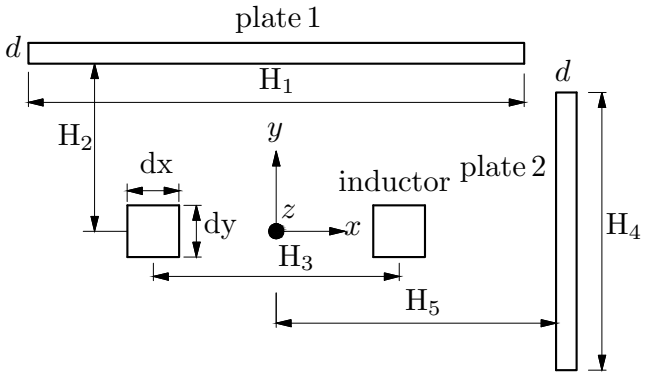

Fig. 4. 2-D geometry of an inductor and two plates (d = 5 mm, H_1 = 120 mm, H_2 = 45 mm, H_3 = 45 mm, H_4 = 80 mm, H_1 = 67.5 mm, dx = dy =12 mm).

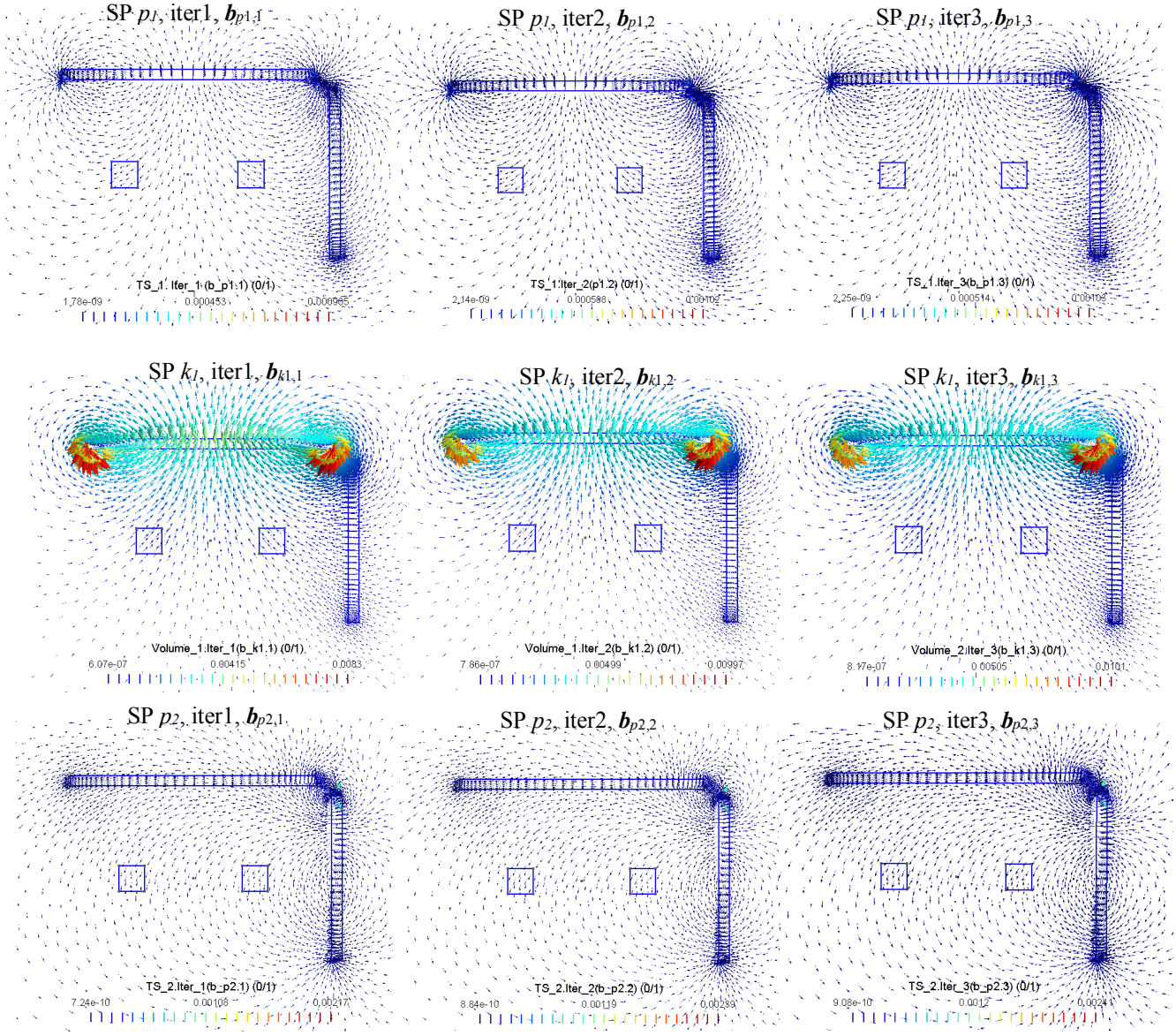

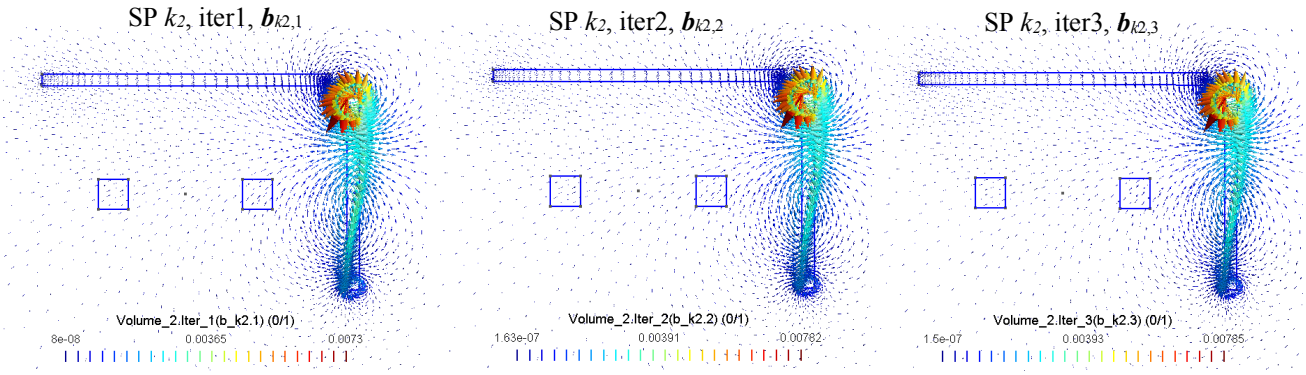

Fig. 5. Magnetic flux densities ($\boldsymbol{b}$) (real part) of the z-component calculated in each SP, i.e. SP p_1, SP k_1, SP p_2 and SP k_2, with three iterations. SP p_1 is chosen as the reference of source SP.

$$\xrightarrow{\text{Convergence}} \boldsymbol{b} = \sum_{i \in P} \boldsymbol{b}_i = \boldsymbol{b}_{q,0} + \sum_{j=1}^{12} \boldsymbol{b}_{p1,j} + \sum_{j=1}^{12} \boldsymbol{b}_{k1,j} + \sum_{j=1}^{12} \boldsymbol{b}_{p2,j} + \sum_{j=1}^{12} \boldsymbol{b}_{k2,j}$$

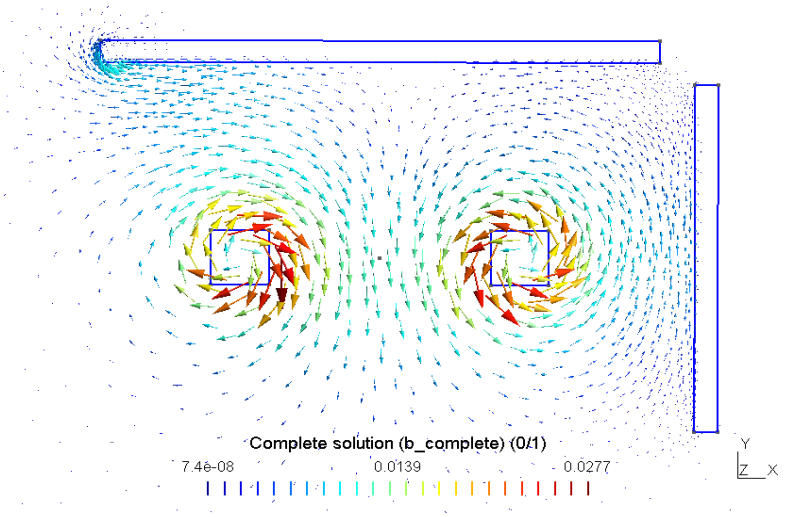

Fig. 6. Convergence complete solution $\boldsymbol{b}$ of SPs at 12 iterations.

An iterative process (with three iterations) of four SPs (i.e. SP p_1, SP k_1, SP p_2 and SP k_2) for the magnetic flux density $\boldsymbol{b}$ is presented in Fig. 5, where SP p_1 is considered as a source for other SPs. It worths noting that the source problem SP q does not need to be corrected, because it only contains the current driven inductor and needs no SS nor VS. The accurate solution gives the tolerance of the complete solution $\boldsymbol{b}$ of the convergence (8 iterations) (Fig. 6). The convergence of the volume correction SP k_2 on the norm of eddy current $\|\boldsymbol{j}\|$ along the plate 1, for different iterations is represented in Fig. 7. The TS solution SP p_2 is also shown as a function of the number of iterations. The computed result of the volume correction SP k_2 along the plate 1 checked to be close to the reference solution is then presented.

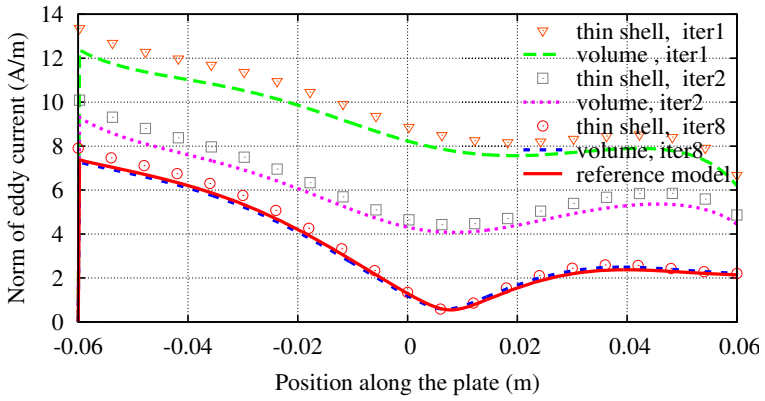

Fig. 7. Norm of eddy current density $\|\boldsymbol{j}\|$ (A/m) along the plate 1 at different iterations (f = 50 Hz, $\mu_r = 1, \sigma = 59$ MS/m).

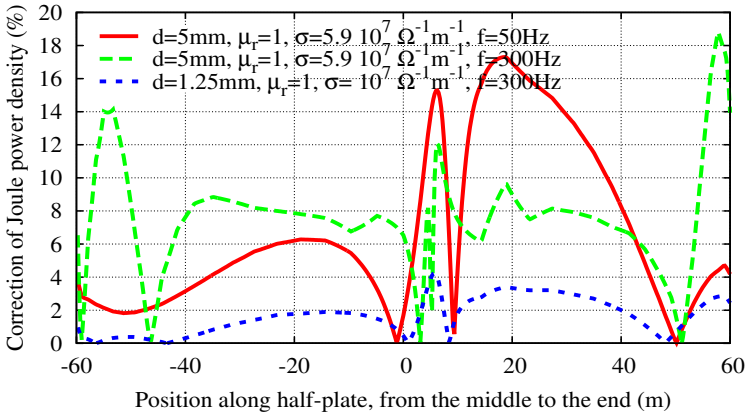

Fig. 8. Relative correction of the Joule power density along the plate 1, with effects of d, μ_r, σ and f.

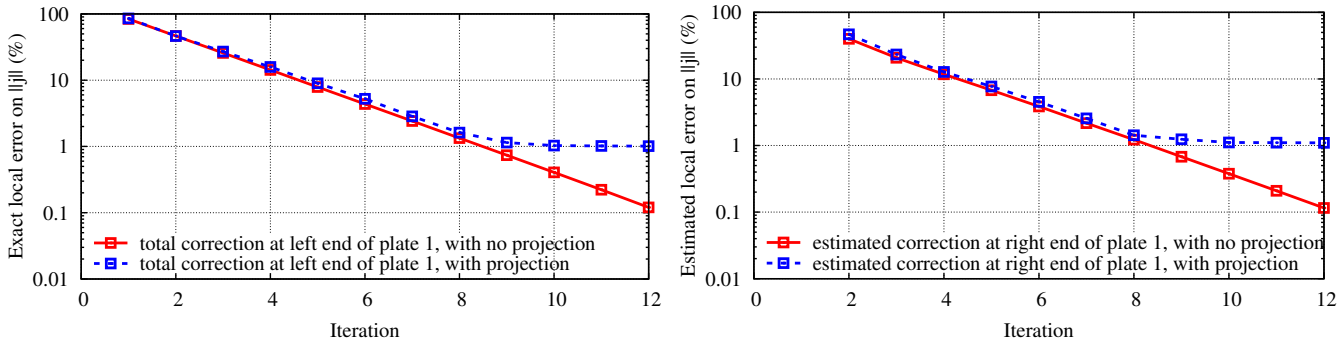

Fig. 9. Exact local errors on the norm of eddy current density $\|\boldsymbol{j}\|$ between the total solution and the reference solution at right end of plate 1 (*left*), and estimated local errors on the norm of the eddy current density $\|\boldsymbol{j}\|$ between the solution at iteration n and n-1, at right end of plate 1 (*right*), for both no projection and projection.

The TS error on the Joule power density in the plate 1 depends on several parameters, as depicted in Fig. 8. It can reach 30% in the end of the plate. Relative local errors on the norm of eddy current density $\|\boldsymbol{j}\|$ between the total solution and the reference solution at the right end of plate 1 are shown in Fig. 9 (*left*). The error is less than 1 % with no projection, and increases slightly up to 1.17 % with projection error, after 12 iterations for both cases.

Estimated local errors on the norm of eddy current density $\|\boldsymbol{j}\|$ between the SP solution at iteration n and the solution at previous iteration n-1 at right end of plate 1 is pointed out in Fig. 9 (*right*), for both cases (no projection and projection). The global errors with projection and no projection on the norm of the magnetic flux density $\boldsymbol{b}$ are eventually illustrated in Fig.10. The errors are below

1% after 12 iterations. The projection error is also approximately 1%. The values of exact and estimated local errors at right end of plate 1 are pointed out in Table I, for both no projection and projection.

The errors on the power loss densities of TS SP p_1 along the plate 1, with different positions of the plate, are indicated in Fig. 11. For a distance between the plate and the inductor $D = H_2/2$ (H_2 is given in Fig. 4), the error on the TS SP p_1 reaches 25% near the plate ends (δ = 3.78 mm) or 89% with skin depth (δ = 2.25 mm) (Fig. 11, *top*), with d = 5mm for both cases. For $D = 2H_2$, it reaches 22% near the plate end (δ = 3.78mm) or 85% with (δ = 2.25 mm) (Fig. 11, *bottom*), with d = 5 mm for both cases.

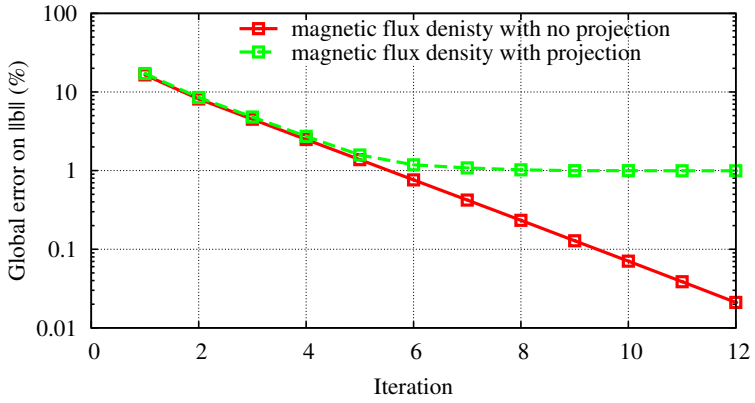

Fig. 10. Global errors on the norm of magnetic flux density $\|\boldsymbol{b}\|$ between the total solution and the reference solution, with the number of iterations.

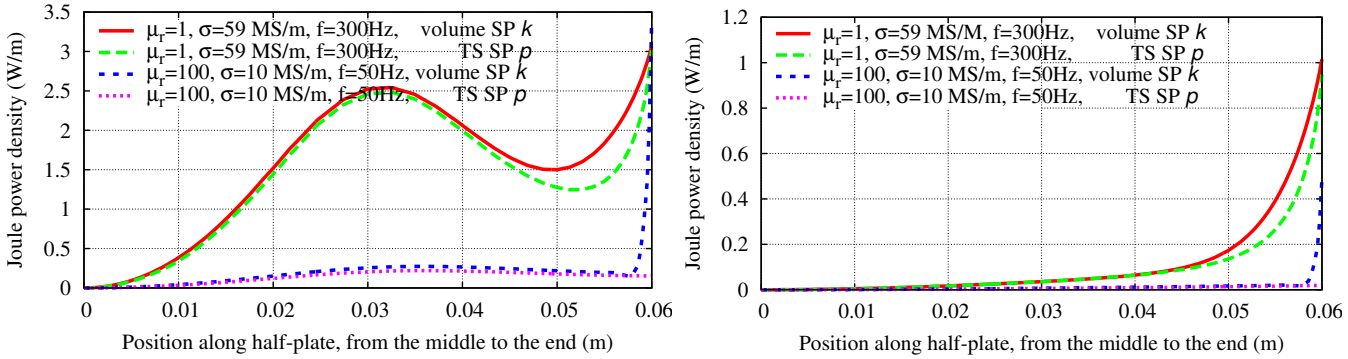

Fig. 11. Power loss density with TS and volume correction along the plate 1 with two positions of a 5 mm thickness plate D = $H_2/2$ (*left*), for D = $2H_2$ (*right*, with H_2 is given in (Fig. 4)).

Table I: Values of exact and estimated local errors at right end of plate 1, for both no projection and projection.

Iteration n	No projection (same mesh)		No projection (same mesh)	
	Exact local error (%)	Estimated local error (%)	Exact local error (%)	Estimated local error (%)
1	91.13	91.13	95.31	91.13
2	49.94	40.5	51.83	43.15
3	27.35	20.81	28.81	21.60
4	15.06	11.76	16.02	11.91
5	8.36	6.76	9.15	7.13

6	4.65	3.86	5.17	4.19
7	2.59	2.17	2.71	2.36
8	1.45	1.23	1.78	1.32
9	0.81	0.67	1.35	1.14
10	0.44	0.37	1.23	1.03
11	0.242	0.21	1.14	1.02
12	0.133	0.12	1.12	1.01

6 Conclusion

In this paper, the convergence of local and global solutions in SPs are successfully obtained in a two-way coupling. Errors on the local and global in SPs have studied, with check of convergence. In particular, SPs in the iterative SPM permits users to use previous solutions for new SPs (variation of geometrical and physical data) instead of solving a new complete problem for each new set of parameters. This iteration could be also accelerated (to reduce the number of iterations), e.g. by extrapolation or by using Krylov subspace techniques [9], [10].

REFERENCES

[1] C. Geuzaine, P. Dular, and W. Legros, "Dual formulations for the modeling of thin electromagnetic shells using edge elements," IEEE Trans. Magn., vol. 36, no. 4, pp. 799--802, 2000.

[2] Tsuboi, H. Asahara, T. Kobaysashi, F. and Misaki, T. (1997), "Eddy current analysis on thin conducting plate by an integral equation method using edge elements" IEEE Trans. Magn., vol. 33, No. 2, pp. 1346-9.

[3] P. Dular, Vuong Q. Dang, R. V. Sabariego, L. Krahenbuhl and C. Geuzaine, "Correction of Thin Shell Finite Element Magnetic Models via a Subproblem Method," IEEE Trans. Magn., vol. 47, no. 5, pp. 1158--1161, 2011.

[4] Vuong Q. Dang , P. Dular, R. V. Sabariego, L. Krahenbuhl and C. Geuzaine, "Subproblem Approach for Thin Shell Dual Finite Element Formulations," IEEE Trans. Magn., vol. 48, no. 2, pp. 407--410, 2012.

[5] P. Dular, L. Krahenbuhl, R.V. Sabariego, Mauricio Ferreira da Luz, Patrick Kuo-Peng, and C. Geuzaine, "A Finite Subproblem Method for Position Change Conductor Systems," IEEE Trans. Magn., vol. 48, no. 2, pp. 403--406, 2012.

[6] P. Dular, and R.V. Sabariego "A perturbation method for computing field distortions due to conductive regions with h-conform magnetodynamic finite element formulations," IEEE Trans. Magn., vol. 43, no. 4, pp. 1293-1296, 2007.

[7] P. Dular, R. V. Sabariego, M. V. Ferreira da Luz, P. Kuo-Peng and L. Krahenbuhl "Perturbation Finite Element Method for Magnetic Model Refinement of Air Gaps and Leakage Fluxes," IEEE Trans. Magn., vol. 45, no. 3, pp. 1400-1403, 2009.

[8] C. Geuzaine, B. Meys, F. Henrotte, P. Dular and W. Legros "Perturbation Finite Element Method for Magnetic Model Refinement of Air Gaps and Leakage Fluxes," IEEE Trans. Magn., vol. 35, No. 3, pp. 1438-1441, 1999.

[9] C. Geuzaine, A. Vion, R. Gaignaire, P. Dular, and R. V. Sabariego"An amplitude finite element formulation for multiple-scattering by a collection of convex obstacles," IEEE Trans. Magn., vol. 46, no. 8, pp. 2963-2966, 2010.

[10] A. Vion, R. V. Sabariego and C. Geuzaine "Model reduction Algorithm for solving multiple-scattering problems using iterative methods," IEEE Trans. Magn., vol. 47, no. 5, pp. 1470-1473, 2011.

[11] Dang Quoc Vuong "Modeling of Electromagnetic Systems by Coupling of Subproblems- Application to Thin Shell Finite Element Magnetic Models," Ph.D. theis, University of Liege, Belgium, Faculty of Applied Sciences, June 2013

Biographies

Dang Quoc Vuong was completed his Ph.D thesis at the University of Liege, Belgium since 2013. He is currently working as a lecturer of School of Electrical Engineering, Hanoi, University of Science and Technology (e-mail: vuong.dangquoc@hust.edu.vn).

Christophe Geuzaine is a full professor at the University of Liege. He is currently working as a head of Electrical Engineering and Computer Science Department of the University of Liège, Belgium, and he is also an official member of the IEEE (e-mail: c.geuzaine@ulg.ac.be).